Nano Research 2017, 10(5): 1804–1818
DOI 10.1007/s12274-017-1505-7
Research Article

ISSN 1998-0124
CN 11-5974/O4

Scanning electron microscopy imaging of single-walled carbon nanotubes on substrates

Dongqi Li[1], Jin Zhang[1], Yujun He[2,3], Yan Qin[4], Yang Wei[1] (✉), Peng Liu[1], Lina Zhang[1], Jiaping Wang[1,5], Qunqing Li[1,5], Shoushan Fan[1,5], and Kaili Jiang[1,5] (✉)

[1] *State Key Laboratory of Low-Dimensional Quantum Physics, Department of Physics and Tsinghua-Foxconn Nanotechnology Research Center, Tsinghua University, Beijing 100084, China*
[2] *Sunwoda Electronic Co. Ltd., Shenzhen 518108, China*
[3] *Graduate School at Shenzhen, Tsinghua University, Shenzhen 518055, China*
[4] *Carl Zeiss Shanghai Co., Ltd. Beijing Office, No. 1221, North Area, Building B, 768 Creative Industry Park, A-5 Xueyuan Rd., Haidian Dist., Beijing 100083, China*
[5] *Collaborative Innovation Center of Quantum Matter, Beijing 100084, China*

Received: 14 November 2016
Accepted: 31 January 2017

© Tsinghua University Press and Springer-Verlag Berlin Heidelberg 2017

KEYWORDS

single-walled carbon nanotube,
scanning electron microscopy,
imaging,
surface charging

ABSTRACT

Scanning electron microscopy (SEM) plays an indispensable role in nanoscience and nanotechnology because of its high efficiency and high spatial resolution in characterizing nanomaterials. Recent progress indicates that the contrast arising from different conductivities or bandgaps can be observed in SEM images if single-walled carbon nanotubes (SWCNTs) are placed on a substrate. In this study, we use SWCNTs on different substrates as model systems to perform SEM imaging of nanomaterials. Substantial SEM observations are conducted at both high and low acceleration voltages, leading to a comprehensive understanding of the effects of the imaging parameters and substrates on the material and surface-charge signals, as well as the SEM imaging. This unified picture of SEM imaging not only furthers our understanding of SEM images of SWCNTs on a variety of substrates but also provides a basis for developing new imaging recipes for other important nanomaterials used in nanoelectronics and nanophotonics.

1 Introduction

The semiconductor industry has entered the nanotechnology era. The top-down approach has been used to fabricate devices with feature sizes approaching the typical size of nanomaterials synthesized by the bottom-up approach. In both approaches, when the size of the nano-units is reduced, the bandgap of the nanomaterials strongly depends on their dimensions. For example, as a typical one-dimensional (1D) nanomaterial, single-walled carbon nanotubes (SWCNTs) can be either metallic or semiconducting depending on their chiral indices, and the bandgap of semiconducting SWCNTs is inversely proportional to their diameters

Address correspondence to Yang Wei, WeiYang@tsinghua.edu.cn; Kaili Jiang, JiangKL@tsinghua.edu.cn

TSINGHUA UNIVERSITY PRESS Springer

[1]. Thus, to fabricate devices with uniform performance for the semiconductor industry, the precise control of the dimensions of the nano-units is required. Additionally, a high-throughput method is imperative for evaluating the distributions of the dimensions and the physical properties, such as the bandgap.

Scanning electron microscopy (SEM) is one of the most frequently used methods for characterizing nanomaterials with a high spatial resolution and high efficiency. However, owing to the finite size of the electron beam, SEM cannot reveal the precise dimensions of nanomaterials with diameters around 1 nm. Recently, without knowing the precise dimensions, we easily discriminated metallic and semiconducting SWNCTs on an insulating substrate using SEM [2]. If the SWCNTs are connected to metallic electrodes, the bandgap distributions can also be clearly observed via SEM [3]. These findings clearly indicate that the substrate plays a vital role in evaluating the physical properties of nanomaterials.

Herein, we present a systematic study on the SEM imaging mechanism of SWCNTs on different substrates. The effects of the acceleration voltages, magnification, dwell time, etc. are carefully investigated. The results indicate that the surface charge and material play key roles in SEM imaging with a variety of frequently used substrates, including conductive substrates, insulating substrates, and insulator-coated conductive substrates. By carefully tuning the imaging conditions and selecting the substrate materials, SEM images with physical-property (e.g., bandgap) contrast are obtained, which is helpful for evaluating the distribution of the physical properties for the various nanomaterials used in nanoelectronics and nanophotonics.

2 Overview of SEM imaging

We begin with a brief review of the operating principle of SEM. Figure 1(a) shows a schematic of the SEM structure. The electron beam emitted from the cathode tip is accelerated and focused by the anode and magnetic lens, respectively. The focused electron beam scans the specimen point-by-point via scanning coils. The secondary electrons (SEs) are produced by the electron bombardment and collected by the SE detector sequentially [4]. The imaging using the SE signals is called the SE mode of SEM.

The SE mode is the most commonly used mode and produces a grayscale image, with the gray value representing the intensity of the SE signal. Such an SEM image contains the surface information, including the topography, the material, and the local surface charge. These three factors significantly affect the SE emission, as shown in Fig. 1(b).

The acceleration voltage, dwell time, and magnification are the most important parameters for SEM imaging. The acceleration voltage determines the energy or wavelength of the incident electrons. A lower acceleration voltage (LV) leads to a longer wavelength, and a higher acceleration voltage (HV) leads to a

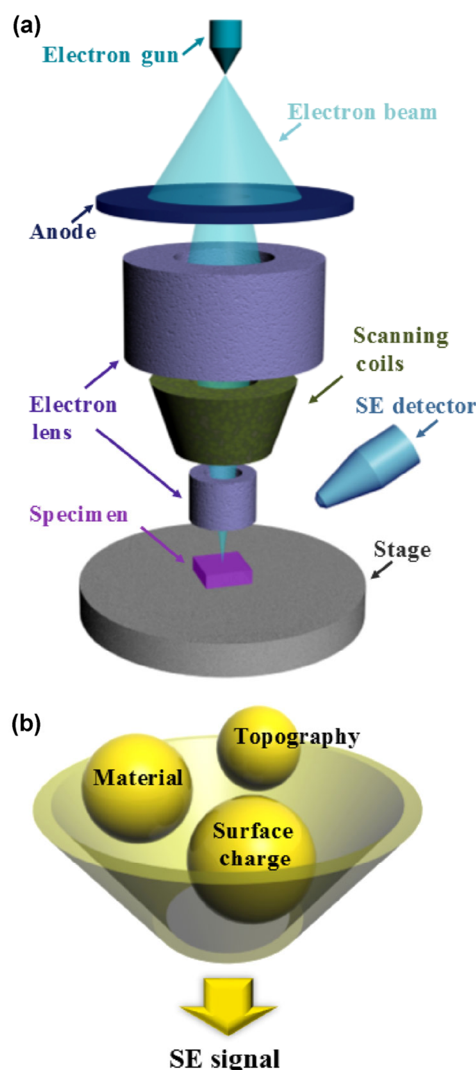

Figure 1 Schematic of the SEM structure and SE signal. (a) Illustration of the SEM structure. (b) Schematic of the information in the SE signal.

shorter wavelength. The spatial resolution of SEM depends on both the wavelength and the entire electron optics system. The acceleration voltage also affects the penetration depth of the incident beam, which is larger for the HV. Two other parameters that affect the imaging, which are less noticed, are the dwell time and the magnification. During normal SEM scans, the focused electron beam is positioned at one spot and remains there for a short period (which is defined as the dwell time). It then moves to the next spot and remains there for the same period, and so on. Thus, the SEM image is generated pixel-by-pixel. Usually, the number of pixels in one scanning line is constant; thus, magnification determines the step length between two adjacent spots. A shorter step length means that the scan is closer to a continuous scan, whereas a longer step length leads to an array of isolated spots. The three kinds of SE signals shown in Fig. 1(b) can be modulated according to these parameters.

The SEs have a low energy (<50 eV) and are released by the inelastic scattering. They are produced along the path of the incident electrons, as shown in Fig. 2(a). Only a small amount of the SEs near the surface can escape, and the escape depth is a few nanometers. The incident electrons dissipate mainly as the specimen currents and backscattering electrons (BSEs), which have a high energy. The SE induced directly by the incident electrons is called SE1, and the emission produced by the BSEs is called SE2. The material signal is caused by the different scattering ability of the atoms; thus, the material signal is produced by both SE1 and SE2. However, the material signal showing the atomic-number contrast is mainly encoded in SE2, as the amount of BSE is more sensitive to the atomic number of the specimen [5]. Heavy elements backscatter electrons more strongly than light elements; thus, the areas corresponding to heavier elements have a brighter color, and vice versa. Because the spatial spread of the BSEs, as well as SE2, is larger than SE1, as shown in Fig. 2(a), the spatial resolution is always lower than the magnitude of the spot size of the incident beam. Schematics of SE1 and SE2 in the LV and HV cases

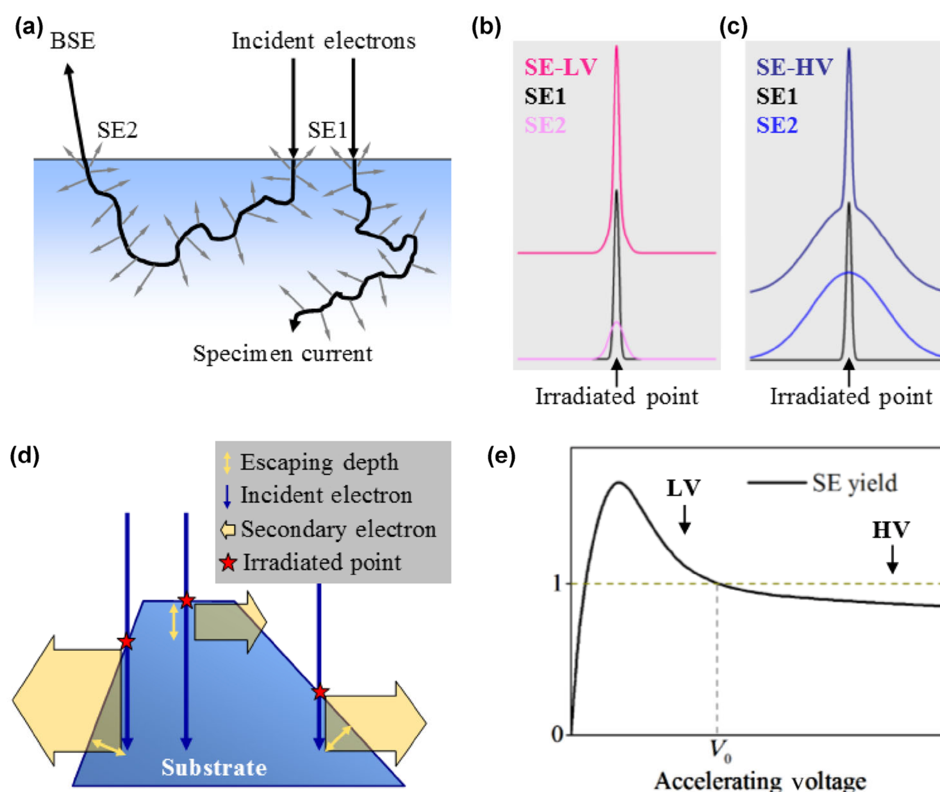

Figure 2 (a) Schematic of BSE, SE1, and SE2. (b) and (c) Spatial distribution of SE1 and SE2 and the total SE yield in the LV and HV cases, respectively. (d) Schematic of the relationship between the surface gradient and the amount of SEs. (e) SE yield curve according to the acceleration voltage.

are shown in Figs. 2(b) and 2(c), respectively. As the acceleration voltage increases, the amount of BSEs also increases. Furthermore, they escape farther away from the irradiated point, which degrades the spatial resolution. Comparing the radius of the SE area with the step size is an effective method for evaluating the spatial resolution. However, in the HV case, where the magnification is so large that the scanning step length is shorter than the radius of the SE2 area, the SE2 signal can be viewed as an even background for each point, and the contrast mainly arises from SE1. SWCNTs are usually observed in this condition because of their nanoscale diameter.

The topography information encoded in SE1 gives rise to a higher spatial resolution, as SE1 is generated within an area very close to the irradiated spot. The escape depth is constant for a specific material; thus, a point with a larger gradient generates more SEs because of the larger escaping area [6], as shown in Fig. 2(d).

The surface-charge distribution also affects the SEM imaging, as the SEs are of such a low energy that they are easily disturbed by the localized electric field. The positive charge pulls the SEs back to the specimen, causing less SEs to reach the SE detector. Thus, the image has a smaller gray-level value and appears darker. In contrast, the negatively charged area exhibits a brighter color. This is confirmed by the acceleration voltage-dependent SE yield of bulk materials (Fig. 2(e)), which is defined as the number of SEs emitted per incident electron. As the acceleration voltage increases, the SE yield increases from zero to a peak value (>1) and then monotonically decreases to <1. In the monotonically decreasing interval, the positively charged area increases the incident beam energy, which is equivalent to a higher acceleration voltage, resulting in a smaller SE yield and thus a darker area in the SEM image. The voltage at the peak value of the SE yield is <1 kV for most materials, and the acceleration voltage for normal SEM is usually within the range of 1–15 kV. Therefore, it is reasonable to only discuss the monotonically decreasing part of the SE yield curve. Here, the LV and the HV are defined as the voltage ranges below and above V_0, respectively, as shown in Fig. 2(d).

The substrate on which the nanomaterials are loaded is essential in the SEM imaging because the surface charge generated on the surface of the substrate significantly affects the material signal from the single-atomic-layer SWCNT walls. On the other hand, the incident-beam size is very close to the diameter of the as-grown SWCNTs, resulting in a very weak material signal. As shown in all the panels in Fig. 3, in the LV case, the positive charge is on the superficial surface. This is because the penetration depth of the incident electrons and the escape depth of the SEs are similar, and the SE yield is >1. In the HV case, the penetration depth of the incident electrons is substantially larger, and the negative charge accumulates near the end of the path. However, the superficial surface is slightly positively charged owing to the SE emission. As shown in Fig. 3, there are three main categories of substrates: the conductive substrate, insulating substrate, and insulator-coated conductive substrate. The surface

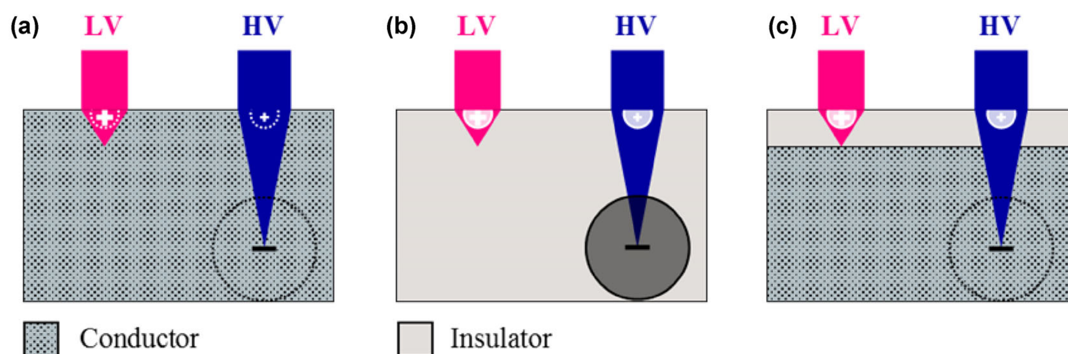

Figure 3 Charging condition of the three categories of substrates irritated by electron beams. The positive charge is generated at the left of the SEs, and the negative charge is generated by the implantation of the incident electrons. (a) For the conductive substrate, a small charge is reserved for both the LV and HV. (b) For the insulating substrate, the charge amount is large, and the total charge is opposite for the LV and HV. (c) Composite substrate is positively charged in both cases, and the charge amount is larger for the LV.

charge depends on both the acceleration voltage and the conductivity of the substrate. For the conductive substrate, the charge can be conducted into the ground quickly; thus, the substrate is nearly charge-neutral when both the LV and HV are applied, as shown in Fig. 3(a). Figure 3(b) shows that the charge is trapped in the insulated substrate, which is thus positively charged in the case of LV and negatively charged in the case of HV. The insulator-coated conductive substrate, as shown in Fig. 3(c), is positively charged in both cases. The incident electrons penetrate the thin insulator and are conducted away in the HV case [7]. Moreover, the surface charging on the insulator-coated substrate is more intensive in the LV case than in the HV case.

3 Experimental

We used SWCNTs on different substrates as model systems to investigate the SEM imaging of nanomaterials. The horizontally aligned SWCNT arrays were synthesized on a stable temperature (ST)-cut quartz substrate via chemical vapor deposition [8]. The SWCNT arrays were transferred onto different target substrates using the poly(methyl methacrylate)-assisted transfer technique [9, 10]. The SWCNTs were parallel to each other, and the alignment was maintained after the transfer process.

SWCNT imaging was performed with the three aforementioned types of substrates. In addition to the ST-cut quartz where the SWCNTs were grown, two additional substrates were employed to represent the other two cases. An SiO_2/Si substrate and the metallic electrodes on the SiO_2/Si were selected as the insulator-coated substrate and the conductive substrate, respectively. These substrates are all important and typical for various investigations. The SEM imaging of SWCNTs on ST-quartz is essential for the study of their growth. The SiO_2/Si wafer and the metallic electrodes on it are widely used in SWCNT devices.

The 300-nm-thick SiO_2 layer was formed by thermal oxidation. The metals were deposited by conventional electron-beam (e-beam) evaporation and a liftoff process. The substrate was annealed at 300 °C in Ar for 30 min to remove the lithography residue before the SWCNTs were transferred.

Two scanning electron microscopes were used to perform the SEM observations: FEI Nova NanoSEM 450 and Zeiss Merlin. The FEI microscope was employed for most of the studies. The spot size was set at 3.5, and the dwell time was 10 μs unless otherwise specified. The Zeiss Merlin successfully performed the LV SEM observations with a high spatial resolution because of its innovative electron optics designed for the LV case. The spot size was set as 1, and the dwell time was 50 ns. The acceleration voltages were set as 1 and 10 kV for the LV and HV cases, respectively. Systematic SEM observations were performed on SWCNTs on different substrates under both the LV and HV.

4 Results

Our previous studies clearly indicate that the substrate plays a vital role in evaluating the physical properties of nanomaterials. Therefore, in the present study, we used SWCNTs as model system to perform SEM on nanomaterials and nanodevices on substrates.

Without a substrate, for example, SWCNTs suspended over a trench, the SE signals detected are nothing but SE1. Unfortunately, the corresponding SEM image does not show any conductivity- or bandgap-dependent contrast. The substrate introduces noise to the SEM images because it causes disturbance. Furthermore, it facilitates the SEM imaging of SWCNTs at a low magnification and enables imaging with conductivity- and bandgap-dependent contrast, as discussed below.

4.1 SWCNTs on metallic electrodes

SEM imaging on metal surfaces is an essential issue and still lacks detailed investigations, although SWCNT-based devices frequently employ SWCNTs on metallic electrodes. The metal weakens the surface charging induced by e-beam irradiation, which is important for SWCNT imaging via SEM. Without a sufficient surface charge, the SEM observation of SWCNTs on the metallic surface is difficult. Comparative studies revealed that the material signal and the charge signal induced by the contact potential significantly affected the SEM imaging.

As shown in Fig. 4(a), metallic $_{21}$Sc, $_{24}$Cr, $_{22}$Ti, $_{79}$Au, $_{78}$Pt electrodes were sequentially deposited on the SiO_2/Si substrate. The metallic thin films were 55 nm thick, including the adhesion layer of Ti (5 nm). The geometry of this specimen is shown in Fig. 4(b). As the SWCNTs crossed both the SiO_2 surface and the metallic stripes, SEM images of the same SWCNT on both surfaces were simultaneously obtained. In the SEM images of the SiO_2 surfaces, s- and m-SWCNTs were easily discriminated [2, 3]. The SEM observations were performed quickly after the CNT transfer to avoid the oxidization of the metal by the air.

SEM images of as-fabricated metallic stripes are presented in Figs. 4(a) and 4(b), indicating that the gray level depended on the atomic number (material signal). The acceleration voltages were 10 kV (HV) and 1 kV (LV). In the figures, the SEM images with blue and pink frames correspond to the HV and LV, respectively. The Sc, Cr, and Ti stripes are significantly darker than the Au and Pt stripes and provide backgrounds for the SWCNTs with different brightness, and affecting the SEM images of the SWCNTs. Furthermore, the contrast was better in the HV case (Fig. 4(a)). The charging signal, which arose from the contact potential induced by the different work functions between the metal and the SWCNTs, was evaluated. Therefore, two comparative experiments were performed to study the effects of the atomic number and work function of the metals on the SEM imaging. First, Au and Pd, with different atomic numbers (79 and 46, respectively) and similar work functions (5.1 and 5.12 eV, respectively) [11] were studied. The similarity of the work functions eliminated the charging difference between the two specimens. The material signal arising from the metal background dominated the difference between the comparative SEM images. The SEM images of the SWCNTs on Au and Pd at an acceleration voltage of 10 kV are shown in Figs. 4(c) and 4(d), and the orientations of the SWCNTs are indicated by the gray arrows between the two images. The SWCNTs appear black on Au and white on Pd. The atomic number of Pd is smaller

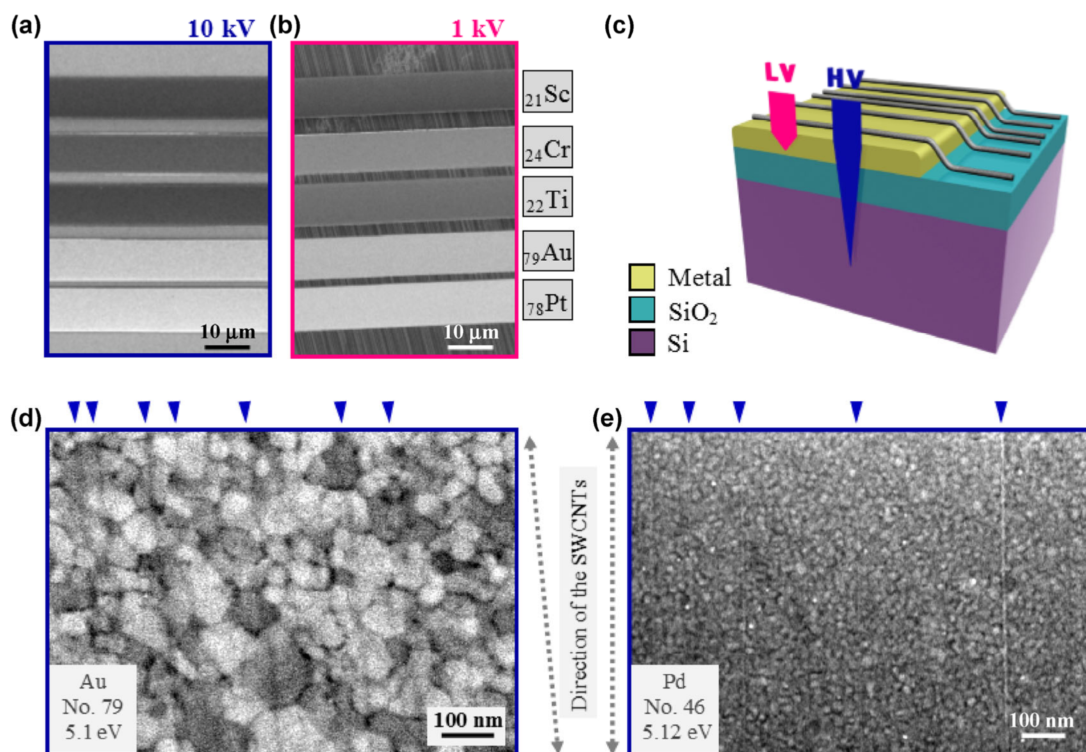

Figure 4 Contrast caused by the atomic number. (a) and (b) SEM images (with acceleration voltages of 1 and 10 kV, respectively) of five kinds of metals. (c) Schematic of the substrate structure used in the experiment. (d) and (e) SEM images (10 kV) of the SWCNTs on Au and Pd, respectively. In the case of the low contrast, the direction of the SWCNTs is labeled by the gray arrows between the two images. The blue triangles at the top mark the location of each SWCNT.

than that of Au; thus, the gray level for Pd was lower. The total yield of the SEs of the SWCNTs was coincidentally between those of Au and Pd. Therefore, the SWCNTs appear to be of opposite colors.

Two other groups of metals with a similar atomic number but significantly different work functions were then selected: $_{78}$Pt (5.65 eV) and $_{79}$Au (5.1 eV), $_{21}$Sc (3.5 eV), and $_{22}$Ti (4.33 eV) [11]. The HV SEM images are shown in Figs. 5(a)–5(d). The upper part of each image shows the SiO_2/Si substrate, and the lower part shows the metal. The orientation of the SWCNTs was adjusted perpendicular to the scanning line. In Figs. 5(a) and 5(b), the SWCNTs on the Pt and Au are black, and the images for the Pt have a far better contrast. The Fermi level of Pt is deeper than that of Au; thus, more electrons flow from SWCNTs to Pt than to Au, causing the SWCNTs to be more positively charged and appear blacker on Pt. Obviously, both m- and s-SWCNTs are observed on the Pt, as both the white and the black SWCNTs on the SiO_2 are visible on the Pt in Fig. 5(a). Both are darker than the substrate. Because the Fermi level of Pt is lower than the valance band edge of the s-SWCNTs, electrons were transferred from the s-SWCNTs to the Pt, resulting in positively charged s-SWCNTs. For Sc and Ti, the SWCNTs on the metals appear white, and the contrast is better for the Sc substrate, as shown in Figs. 5(c) and 5(d). This is ascribed to the Fermi-level difference between the metal and the SWCNTs. The Fermi level of Sc is far higher than that of the SWCNTs; thus, the SWCNTs were more negatively charged. The negatively charged area exhibits a brighter color, and the contrast is better for Sc. Furthermore, most of the s-SWCNTs are almost invisible for the two metals, as the black lines on the SiO_2/Si substrate interrupt at the boundary, as shown in Figs. 5(c) and 5(d). This phenomenon is not well understood and is difficult to interpret, highlighting the need for further studies.

The charging effect under the LV was similar to the HV on these metallic electrodes, and the main difference arose from the surface charge signal. The focus quality of the e-beam was worse in the LV case, which weakens the material signal. The feature of the image for each metal is similar to the aforementioned HV case, as shown in Figs. 6(a)–6(d). The SWCNTs are invisible on Au in the LV case, which means that they were almost charge-neutral on the Au substrate, owing to the nearly identical Fermi levels of Au and the SWCNTs.

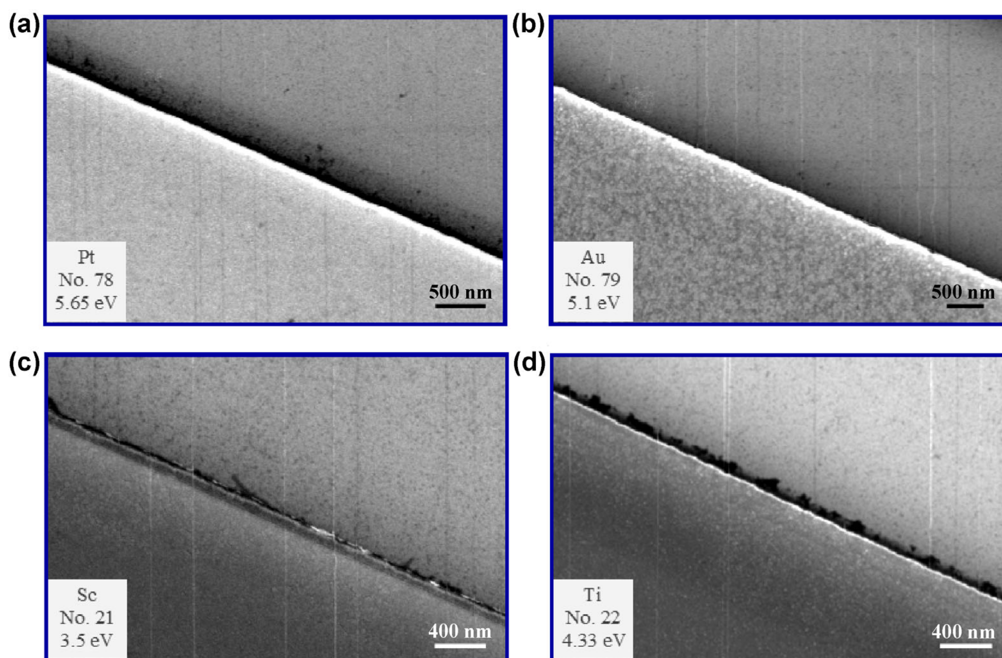

Figure 5 SEM image of the SWCNTs on metals with different work functions in the HV case. (a)–(d) SEM images (10 kV) of the SWCNTs on Pt, Au, Sc, and Ti. The atomic number and work function are labeled in the bottom left of each image. The upper part of each image shows the SiO_2/Si substrate, and the lower part shows the metal.

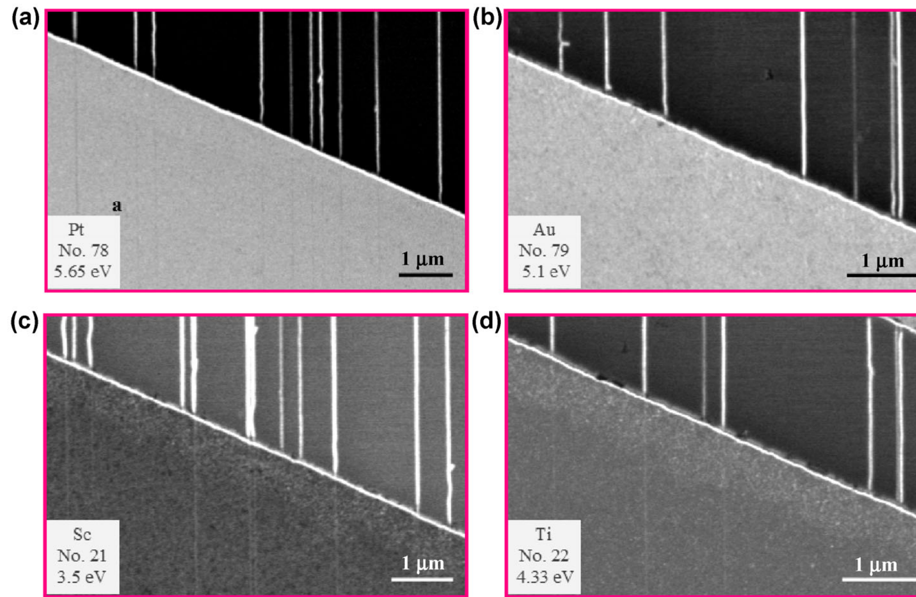

Figure 6 SEM images of the SWCNTs on metals with different work functions in the LV case. (a)–(d) SEM images (1 kV) of the SWCNTs on Pt, Au, Sc, and Ti. The atomic number and work function are labeled in the bottom left of each image. The upper part of each image shows the SiO_2/Si substrate.

4.2 SWCNTs on quartz

Because SWCNT arrays were grown on the ST-cut quartz substrate, quartz was selected to study the SEM imaging on insulated substrates. Unlike the metals, the surface of the insulator was intensively charged by the e-beam irradiation under SEM. The SWCNTs on the surface provided an efficient conducting channel to the ground, which fully or partially neutralized the surface charges in the vicinity of the SWCNTs, resulting in a surface-charge contrast. Therefore, the charging information dominated the SEM imaging, rather than signals due to the topography and materials. The SEM images were obtained at acceleration voltages of 1 and 10 kV, respectively. At the LV, which has been studied in previous works, the SE yield coefficient was >1, which means that there were more SEs than incident electrons and that the substrate was positively charged. The SWCNTs and the area around them obtained electrons from the ground, and the electron supplementation was more efficient for the m-SWCNTs than for the s-ones [3]. Therefore, the images of the SWCNTs on quartz exhibit bright lines with a conductivity-dependent gray level, as shown in Fig. 7(a). This conclusion was confirmed by transport measurements of SWCNT field-effect transistors.

The imaging of SWCNTs on quartz under the HV was further studied. Such investigations are rare in the literature. Figure 7(b) shows an HV SEM image obtained at the same location as that in Fig. 7(a). The density of the SWCNTs should be high enough, and it is better to connect the SWCNTs to the ground. All the SWCNTs appear black in the HV SEM image, and the contrast is completely reversed compared with the LV image, as the m-SWCNTs exhibit darker lines, whereas the s-SWCNTs exhibit grayish lines. To further investigate the difference between the HV and LV SEM images, the widths of the SWCNTs in both images were measured and analyzed statistically. Here, the width was defined as the full width at the half maximum of the averaged gray-level plot. The SWCNTs were aligned perpendicular to the scanning line, and all the images were obtained at a magnification of 40kX with a dwell time of 20 μs. As shown in Fig. 7(c), the results indicate that the average widths in the LV and HV cases were 57.44 and 22.65 nm, respectively. Thus, the HV yielded a higher spatial resolution. Both the reversed contrast and the higher spatial resolution are ascribed to the different SE yields at the HV, as plotted in Fig. 2(d). As the SE yield was <1 in the HV case, the surface of the quartz was negatively

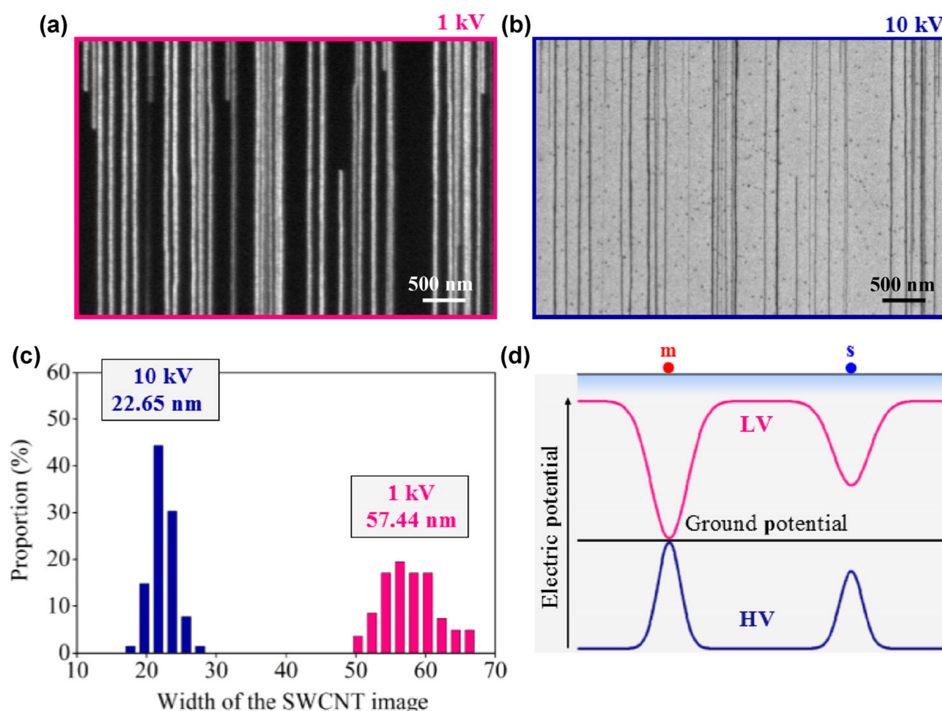

Figure 7 Imaging the SWCNTs directly on the insulated substrate. (a) and (b) SEM images of the SWCNTs on ST-cut quartz obtained at acceleration voltages of 1 and 10 kV, respectively. (c) Bar diagram of the width distribution of the SWCNT images. The average widths were 26.55 in the HV case and 57.44 in the LV case. (d) Schematic of the electric potential of the insulated substrate near the m-/s-SWCNT in the HV and LV cases.

charged, and negative charges (electrons) were conducted to the ground through the conductive SWCNTs array. Therefore, the electron electrical potential near the SWCNTs was lower, reducing the SE yield and causing the SWCNTs to appear black. The m-SWCNTs are brighter than the s-ones in the LV images, as shown in Fig. 7(a) and indicated by the pink curve in Fig. 7(d). Clearly, in the HV case, the m-SWCNTs exhibited a darker color than the s-SWCNTs, as indicated by the blue line in Fig. 7(d). Moreover, the SE yield curve in Fig. 2(d) indicates that the SE yield at the HV had a smaller deviation from 1 than that at the LV, indicating the smaller amount of charge on the surface in the HV case for the same dwell time. Thus, the HV SEM image had a higher spatial resolution.

Using another method, i.e., the conventional preparation of the insulating specimen, a thin layer of metal was deposited on SWCNT/quartz to make the surface conductive and allow the accumulated surface charge to disperse. In general, the metallic coating works because it not only eliminates the surface charging but also inherits the topography of the raw specimen. The advantage of the metal layer is that the topography signal is increased because the scattering capability of the metal deposits is stronger than that of the two walls of the SWCNTs. Because the diameter of the SWCNTs was so small (~1 nm), the surface may have been smoothed after the metal deposition, making the SWCNTs invisible. However, we clearly observed the SWCNTs after a film of 2-nm Cr and 50-nm Pt was deposited on the quartz substrate via an e-beam evaporator, as shown in the SEM image in Fig. 8(a), even though the thickness of the metal layer was far greater than the diameter of the SWCNTs. AFM was performed to confirm that the contrast of the SEM image arose from the topography signal. Regarding the possible piezoelectricity on quartz, AFM was performed on an SiO_2/Si substrate onto which the SWCNTs were transferred. The AFM image (Fig. 8(b)) and the comparative profile plots (Fig. 8(c)) clearly indicate that the topographical information of the SWCNTs was well reserved on the metal surface. A uniform growth mode was observed during the

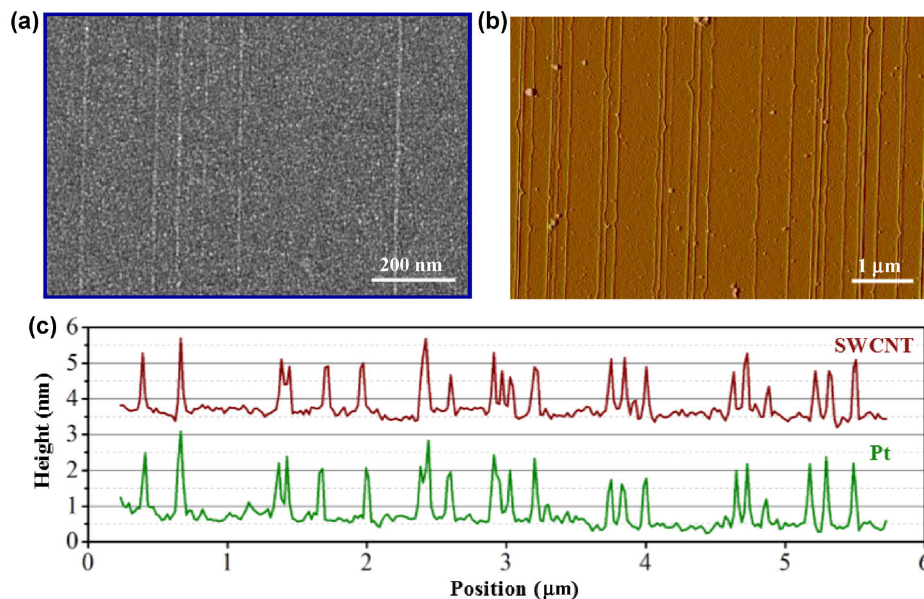

Figure 8 (a) SEM image of the Pt-coated SWCNTs on ST-cut quartz. (b) Atomic force microscopy (AFM) image of the Pt-coated SWCNTs on the SiO_2/Si substrate. (c) AFM profile plots of the SWCNT array on the SiO_2/Si substrate without (brown line) and with (green line) the Pt coating.

thin-film deposition. The substrate was kept at a low temperature in the e-beam deposition; thus, the metal particles did not move or fuse. The bulges on the metal surfaces were only ~1 nm high, showing a bright topography contrast compared with the metal surface. The enhanced SE signals arising from the bulges were due to the larger surface area from which the SEs escaped, compared with the flat surface. The method of metal film coating was efficient for the SEM characterization of the horizontally aligned SWCNT arrays with a low and high density.

4.3 SWCNTs on SiO_2/Si substrate

SiO_2/Si substrates are commonly used in SWCNT devices. They are always positively charged in both the HV and LV modes of SEM, as discussed in Section 2. For the LV case on an SiO_2/Si substrate, the surface charging is similar to that on an insulating substrate, because most of the incident electrons are stopped in the thin SiO_2 layer, as illustrated in Fig. 3(c). All the SWCNTs on the SiO_2/Si substrate appear as bright lines, and the m-SWCNTs have a higher gray level, as shown in Fig. 9(a). However, coincidentally, a thin black line was observed in the middle of each SWCNT at a high magnification of ≥50kX using another scanning electron microscope (Zeiss Merlin), as shown in Figs. 10(a) and 10(b). In the LV case, the quartz substrate behaved identically to the SiO_2/Si substrate; consequently, black thin lines are also observed in the SEM images of the SWCNTs on quartz (Figs. 10(c) and 10(d)).

The thin black line long confused us, until our recent progress on the SEM imaging of SWCNTs on SiO_2/Si in the HV case [12]. In the HV case, the s-SWCNTs appear darker, and the m-SWCNTs appear brighter than the substrate, as shown in the SEM image of Fig. 9(b), which was obtained at the same location as that of Fig. 9(a). The substrate was also positively charged in the HV case; thus, the surface-charge signal indicated that the SWCNTs were brighter than the substrate. However, the charge amount was lower because of the smaller SE yield in the HV case, as indicated by the curve in Fig. 2(d); thus, the material signal was comparable to the surface-charge signal. The SWCNTs appear darker than the substrate for a pure material signal [12]. The SE signal is the combination of the two signals, as shown in Fig. 11(a). For the m-SWCNTs, which have good conductivity, the surface-charge signal dominated, whereas for the s-SWCNTs, the material signal dominated.

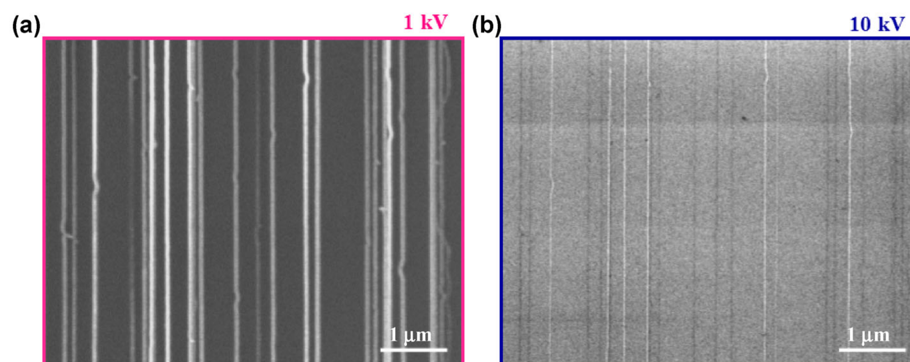

Figure 9 SEM images of the SWCNTs on SiO_2/Si substrate: (a) LV case; (b) HV case.

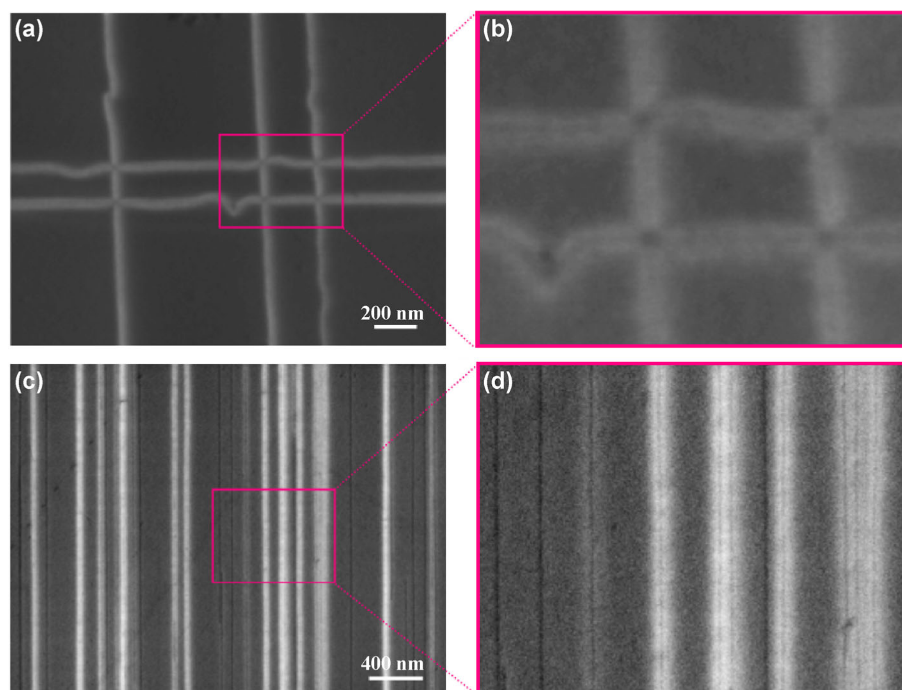

Figure 10 SEM images of the thin black line in the LV case. (a) and (b) SEM images of different magnifications showing the SWCNTs on the Si/SiO_2 substrate. (c) and (d) SEM images of different magnifications showing the SWCNTs on ST-cut quartz.

The material signal is the key reason for the thin black line in the LV case. Generally, the electron beam of SEM has a higher quality in the HV mode than in LV the mode. Thus, the optimal spatial resolution can be achieved only with the HV. To increase the quality of the electron beam in the LV case, some commercial SEMs (e.g., ZEISS Merlin) employ an electrostatic lens at the end of the HV electron column to decelerate the electrons, as shown in Fig. 11(b). Such a low-energy beam has a higher quality, and the SEM has better performance at the LV. The material signal has a far higher spatial resolution than the surface charging signal in the LV case; thus, the better-focused electron beam outlined it with a thin black line, as illustrated in Fig. 11(c).

4.4 Junctions

The junctions formed when SWCNTs contact other materials or structures play an important role in device applications [13–18]. Charge transfer occurs at these junctions owing to the difference in the Fermi levels. The resulting contact-potential difference makes the junctions visible in SEM images.

We previously reported the LV SEM imaging of the

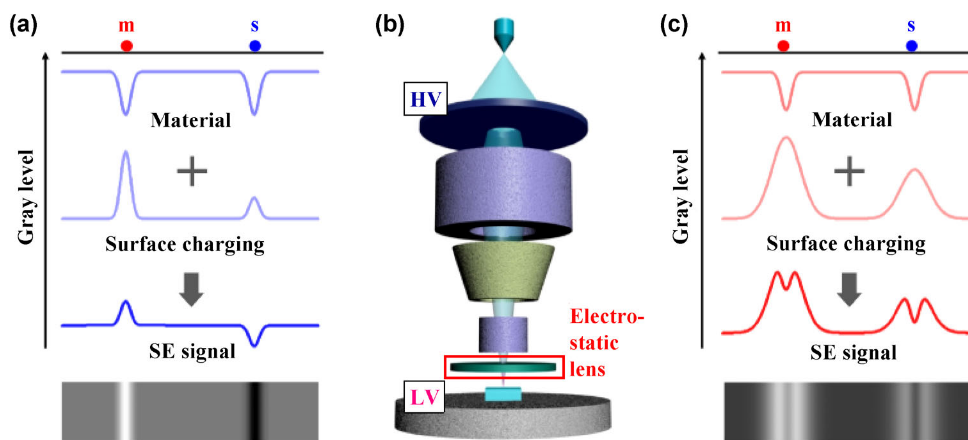

Figure 11 Imaging performed by applying the decelerating voltage. (a) Schematic of the black and white SWCNTs in the HV case on the composite substrate. The inset shows a simulated image of the SWCNTs in this case. (b) Schematic of the application of the decelerating electrostatic lens. (c) Schematic of the emergence of the black thin line in the LV case. The inset shows a simulated image of the SWCNTs in this case.

Schottky barrier at the metal-s-SWCNT contact [3]. It appears as a bright segment up to several micrometers in length because of the space charge distribution in the depletion region. Here, we present the LV and HV SEM imaging of the Schottky barrier at the SWCNT-metal contact, the SWCNT–SWCNT contact, and the p–n junction of SWCNT–two-dimensional (2D) MoS_2. Figures 12(a) and 12(b) show the junction at the SWCNT–Ti contact in the HV and LV modes, respectively. The bright segment along the s-SWCNT at the contact represents the depletion regions, and the length is inversely proportional to the bandgap of the s-SWCNTS. The identification of the depletion region was upgraded from the gray-level difference to the white–black reverse by using the HV. In the SEM images of Figs. 12(c) and 12(d), the bright segment along the s-SWCNTs represents the Schottky barriers at the m- and s-SWCNT contact in both the HV and LV cases. These junctions are more suitable for the bandgap evaluation, as the depletion length can be more efficiently measured without the rough edge of the metal layer. Figures 12(e) and 12(f) show SEM images of the p–n junction at the SWCNT–MoS_2 flake contact in the HV and LV cases, respectively. The depletion regions along the SWCNT side appear as bright segments and are indicated by arrows. However, no apparent depletion area is observed on the MoS_2 side at the contact, which is ascribed to the short length of depletion region.

5 Summary

We used SWCNTs on different substrates as model systems to perform SEM imaging on nanomaterials. The SE intensity is affected by a variety of factors, among which the topography, material, and surface charge are the most important and should be seriously considered.

The topography contrast is displayed in an SEM image if zero-dimensional (0D) or 1D nanomaterials or nanostructures sit on a flat surface of the same material, appearing as bright dots or lines, respectively. The enhanced SE signals are due to the larger surface area of the 0D and 1D nanomaterials from which SEs can escape. The topography signal arises from both SE1 and SE2, and the topography contrast is visible at a height difference as small as 1 nm.

The material signal is also composed of SE1 and SE2 from the nanomaterials. For suspended nanomaterials, only SE1 contributes to the material signal. If the nanomaterial is placed on a substrate, both SE1 and SE2 contribute to the material signal.

The surface-charge signal originates from the surface charge distribution. There are two classes of surface charges. Class I surface charges are caused by the charge transfer due to the difference in the Fermi levels (also reflected by the work function) of two contacting materials, e.g., the surface charges in Schottky barriers, p–n junctions, and contact potential

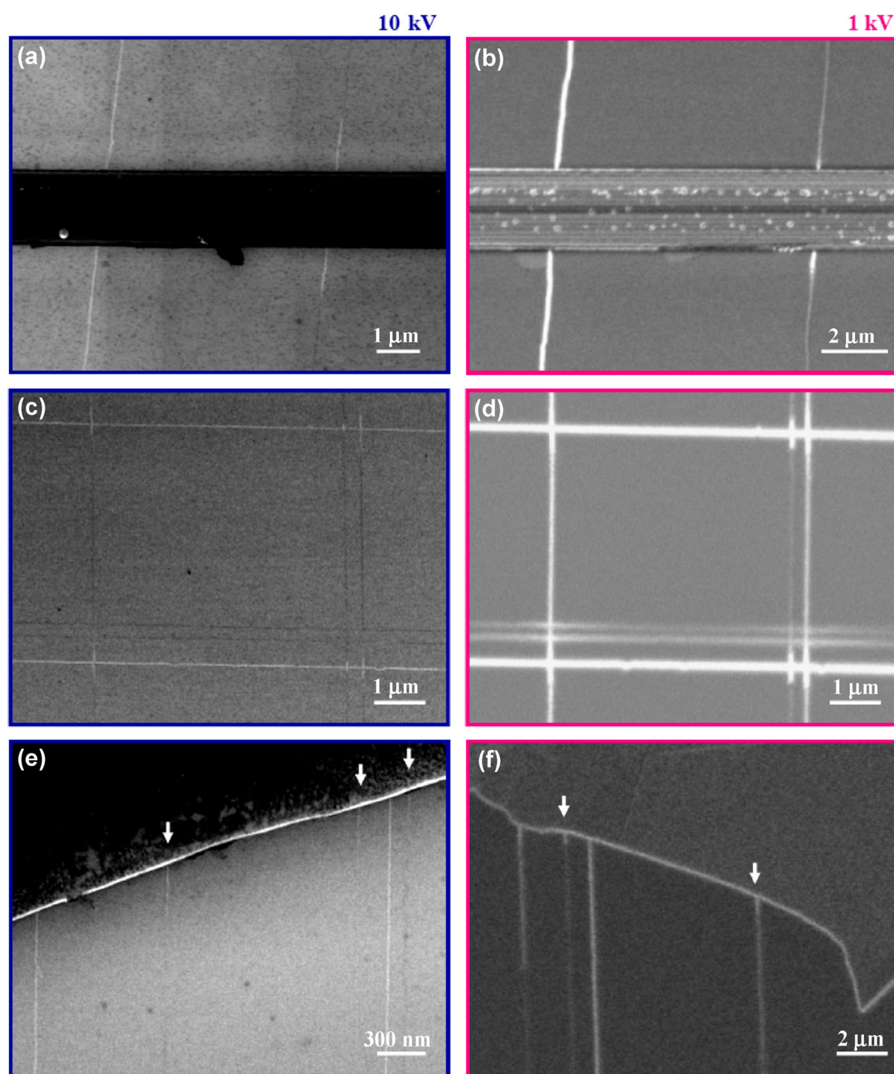

Figure 12 SEM images of the Schottky and p–n junctions on the SiO_2/Si substrate. (a) and (b) SEM images (10 and 1 kV, respectively) of the SWCNTs, which are partly covered with a thin layer of Ti (50 nm). (c) and (d) SEM images (10 and 1 kV, respectively, in the same area) of the crossed SWCNTs. (e) and (f) SEM images (10 and 1 kV, respectively) of the p–n junction between the MoS_2 and s-SWCNTs, indicated by the white arrows.

barriers. Class II surface charges are those induced by e-beam irradiation on insulators. For example, the surface of quartz is positively and negatively charged when irradiated with LV and HV electrons, respectively. The surface charge is more intense in the LV case than in the HV case. This e-beam-induced surface charge results in charge transfer (tunneling) from the nanomaterial to the surrounding area, creating a surface-charge contrast. This second class of surface charge does not exist in the case of a metal substrate.

With these general concepts in mind, we summarize how the substrate and imaging parameters affect the SEM imaging.

The presence of the substrate has several consequences. First, SE1 and SE2 are introduced by the substrate materials. These large signals provide a background for the SEM image, and their fluctuation results in noisy images. Second, the substrate causes BSEs to generate SE2 from the nanomaterials. Finally, it creates a surface charge, providing surface-charge contrast in the SEM images. Metal substrates mainly contribute to the Class I surface charge, whereas insulators mainly induce Class II surface charge.

The imaging parameters, including the beam size, acceleration voltage, dwell time, and magnification, also affect the SEM imaging.

The beam size is very important in the imaging of 0D and 1D nanomaterials. If it is significantly larger than the diameter of 0D and 1D nanomaterials, the SE signals from the nanomaterials are small compared with those from the substrate because the surface area covered by the 0D and 1D nanomaterials is a very small fraction of the e-beam spot area. Therefore, the material signals can only be observed in an SEM image when the beam size is on the same order as the diameter of the 0D and 1D nanomaterials.

The beam size is determined by the acceleration voltage (or wavelength of electrons) in the case of the best focusing and identical electron optics design. Thus, the acceleration voltage also plays important roles in SEM imaging. The first role is determining the wavelength of the electrons and consequently the beam size. The second role is affecting the charging of the insulator surfaces, as previously discussed. An LV causes an intense positive charge on the insulating surface, whereas an HV causes a mild negative charge.

Another parameter that directly affects the charging is the dwell time. Usually, a longer dwell time gives rise to stronger charging.

The magnification has many effects. It determines the step length between adjacent scanning spots. Thus, the first effect is that a smaller magnification may result in nanomaterials being missed during the scanning. The second effect is that the average charging is weak at a low magnification. The third effect is not easily noticed. Under a mild charging condition, the longer step length hinders the tunneling from the nanomaterial to the surrounding area. Thus, little surface-charge contrast appears here. Therefore, the magnification also plays important roles in the surface charging.

Now, we have reached a comprehensive understanding of the effects of the imaging parameters and substrates on the material and surface-charge signals, as well as on SEM imaging. This unified picture is crucial for understanding SEM images of SWCNTs.

For suspended SWCNTs, the SEM image is only composed of the SE1 signal from the nanomaterial and is of a high spatial resolution.

If SWCNTs are placed on substrates, the contrast displayed in an SEM image mainly arises from the material and surface-charge signals. The surface-charge contrast is more easily observed because the collected SEs are from the substrate, which is modulated by the surface-charge distribution and is more intense than the SEs from the nanomaterials. On the other hand, the material contrast is difficult to observe because it arises from the difference in the total yields of the SEs from the nanomaterial and the substrate. This contrast can only be observed when the diameter of the beam spot is very close to the diameter of SWCNTs. Consequently, the material contrast has a higher spatial resolution than the surface-charge contrast.

In the case of an insulating substrate, the surface charge (Class II) is generated everywhere by e-beam irradiation, except in the vicinity of the SWCNTs, where the surface charges are neutralized through tunneling. The width of the charge-neutralized region is larger than the diameter of the SWCNTs, making it visible even at low magnifications. Because the total yield of SEs from the SWCNTs is smaller than that from SiO_2, the material contrast appears as a dark thin line superposed on the surface-charge contrast in SEM images.

If SWCNTs are placed on metal surfaces, charge transfer occurs owing to the difference in the Fermi levels. Charges are stored at the interface between the SWCNTs and the metal substrate, showing a Class I surface-charge contrast in the SEM images. Usually, this contrast has a higher spatial resolution than that for an insulating substrate. The material contrast is superposed on surface-charge contrast and can only be noticed when the Fermi levels are nearly identical.

If SWCNTs are placed on an insulating substrate but connected to other materials, such as metals, m-SWCNTs, or 2D MoS_2, Schottky barriers and p–n junctions are formed at the contact regions, and a Class I surface-charge contrast appears in the SEM image.

In summary, SWCNTs on different substrates were used as model systems to investigate the SEM imaging of nanomaterials. Substantial SEM observations were conducted at both high and low acceleration voltages, leading to a comprehensive understanding of the effects of the imaging parameters and substrates on

the material and surface-charge signals, as well as on the SEM imaging. This unified picture of SEM imaging not only furthers our understanding of SEM images of SWCNTs on a variety of substrates but also provides a basis for developing new imaging recipes for other important nanomaterials used in nanoelectronics and nanophotonics.

Acknowledgements

This work was financially supported by the National Basic Research Program of China (No. 2012CB932301), and the National Natural Science Foundation of China (Nos. 51472142, 51672152, 51472141, 51532008, and 51102147).

References

[1] Saito, R.; Dresselhaus, G.; Dresselhaus, M. S. *Physical Properties of Carbon Nanotubes*; Imperial College Press: London, 1998.

[2] Li, J.; He, Y. J.; Han, Y. M.; Liu, K.; Wang, J. P.; Li, Q. Q.; Fan, S. S.; Jiang, K. L. Direct identification of metallic and semiconducting single-walled carbon nanotubes in scanning electron microscopy. *Nano Lett.* **2012**, *12*, 4095–4101.

[3] He, Y. J.; Zhang, J.; Li, D. Q.; Wang, J. T.; Wu, Q.; Wei, Y.; Zhang, L.; Wang, J. P.; Liu, P.; Li, Q. Q. et al. Evaluating bandgap distributions of carbon nanotubes via scanning electron microscopy imaging of the schottky barriers. *Nano Lett.* **2013**, *13*, 5556–5562.

[4] Wells, O. C. *Scanning Electron Microscopy*; McGraw Hill: New York, 1974; pp 1–6.

[5] Shimizu, R. Secondary electron yield with primary electron beam of kilo-electron-volts. *J. Appl. Phys.* **1974**, *45*, 2107–2111.

[6] Seiler, H. Secondary electron emission in the scanning electron microscope. *J. Appl. Phys.* **1983**, *54*, R1–R18.

[7] Cazaux, J. Some considerations on the electric field induced in insulators by electron bombardment. *J. Appl. Phys.* **1986**, *59*, 1418–1430.

[8] Kocabas, C.; Hur, S. H.; Gaur, A.; Meitl, M. A.; Shim, M.; Rogers, J. A. Guided growth of large-scale, horizontally aligned arrays of single-walled carbon nanotubes and their use in thin-film transistors. *Small* **2005**, *1*, 1110–1116.

[9] Jiao, L. Y.; Fan, B.; Xian, X. J.; Wu, Z. Y.; Zhang, J.; Liu, Z. F. Creation of nanostructures with poly(methyl methacrylate)-mediated nanotransfer printing. *J. Am. Chem. Soc.* **2008**, *130*, 12612–12613.

[10] He, Y. J.; Li, D. Q.; Li, T. Y.; Lin, X. Y.; Zhang, J.; Wei, Y.; Liu, P.; Zhang, L. N.; Wang, J. P.; Li, Q. Q. et al. Metal-film-assisted ultra-clean transfer of single-walled carbon nanotubes. *Nano Res.* **2014**, *7*, 981–989.

[11] Michaelson, H. B. The work function of the elements and its periodicity. *J. Appl. Phys.* **1977**, *48*, 4729–4733.

[12] Li, D. Q.; Wei, Y.; Zhang, J.; Wang, J. T.; Lin, Y. H.; Liu, P.; Fan, S. S.; Jiang, K. L. Direct discrimination between semiconducting and metallic single-walled carbon nanotubes with high spatial resolution by SEM. *Nano Res.*, in press, DOI: 10.1007/s12274-016-1372-7.

[13] Yao, Z.; Postma, H. W. C.; Balents, L.; Dekker, C. Carbon nanotube intramolecular junctions. *Nature* **1999**, *402*, 273–276.

[14] Fuhrer, M. S.; Nygård, J.; Shih, L.; Forero, M.; Yoon, Y. G.; Mazzoni, M. S. C.; Choi, H. J.; Ihm, J.; Louie, S. G.; Zettl, A. et al. Crossed nanotube junctions. *Science* **2000**, *288*, 494–497.

[15] Park, J. W.; Kim, J.; Yoo, K. H. Electrical transport through crossed carbon nanotube junctions. *J. Appl. Phys.* **2003**, *93*, 4191–4193.

[16] Nojeh, A.; Lakatos, G. W.; Peng, S.; Cho, K.; Pease, R. F. W. A carbon nanotube cross structure as a nanoscale quantum device. *Nano Lett.* **2003**, *3*, 1187–1190.

[17] Liu, W.; Hierold, C.; Haluska, M. Electrical contacts to individual SWCNTs: A review. *Beilstein J. Nanotechnol.* **2014**, *5*, 2202–2215.

[18] Dissanayake, D. M. N. M.; Zhong, Z. H. Schottky diodes using as-grown single-walled carbon nanotube ensembles. *Appl. Phys. Lett.* **2014**, *104*, 123501.